J Fusion Energ
DOI 10.1007/s10894-009-9245-7

ORIGINAL PAPER

Simulation of Plasma Focus Devices with Hemisphere Electrodes

M. A. Abd Al-Halim

Abstract A magneto-hydrodynamic simulation of a plasma focus device with hemisphere electrodes is constructed. The snowplow model is used with help of the momentum conservation equation to describe the motion of the plasma sheath between the two concentric hemispheres. The model simulates various plasma parameters like plasma temperature and plasma sheath velocity. The circuit equation is used to calculate the discharge current and electrodes voltage across the two hemisphere terminals. A comparison between the cylindrical and spherical devices is built. The results show that the current dip and the spike voltage is expected to be much pronounced in the spherical devices. It is found also that the plasma sheath velocity and temperature in the case of the cylindrical system are higher than that in the spherical one.

Keywords MHD · Plasma focus · Snowplow model · Hemisphere electrodes

Introduction

A dense plasma focus (DPF) is a device that can generate, accelerate and pinch plasma by electromagnetic forces. The short-lived pinched plasma is sufficiently hot and dense to enhance nuclear fusion reactions, even with high threshold energies, which make it a multi-radiation source. Since the whole discharge lasts few tens of microseconds, the DPF works in pulsed mode and can be efficiently operated in a repetitive regime. The device was independently developed in the early 1960s by Mather [1, 2] and by Filippov [3] in two configuration, which mainly differs basically in the dimension of the inner and the outer electrodes which affect the macroscopic direction of motion of the accelerated plasma.

A Mather type was studied and many models were developed to simulate the plasma motion in both the axial and the radial phases. One of the most interesting models was developed by Lee [4–14]. Lee developed his model of the plasma focus with a complete description of the plasma focus dynamics in the axial and in the radial phases [4, 5]. He obtained a variation in the circuit current with the discharge time and used the shock wave properties to obtain the plasma temperature and the axial shock velocity [5]. The model used the slug model in the radial phase to calculate the radial shock speed and the radial piston speed [4, 6], while the discharge current and voltage across the tube were calculated using the plasma circuit equation [7]. An updated version of this model was proposed by adding the mass and current factors to the model equations. Lee also, was developed a model of the radiative plasma focus by calculating the energy transfer based on the corona model [8]. He added the reflected shock phase and the radiative phase to the model to simulate the X-ray emission [9]. And He was able to calculate the dimensions and the lifetime of the pinch [10, 11]. A recent development is the inclusion of the neutron yield, using a beam–target mechanism [12–14], incorporated in the code resulting in realistic neutron yield scaling with pinch [13]. The versatility and utility of the model is demonstrated in its clear distinction of pinch current from peak discharge current [15] and the recent uncovering of a plasma focus pinch current limitation effect [12, 14].

M. A. Abd Al-Halim
Faculty of Science, Physics Department, Benha University, Benha, Egypt

M. A. Abd Al-Halim (✉)
Department of Nuclear Engineering, North Carolina State University, Raleigh, NC 27695-7909, USA
e-mail: ma_halim74@yahoo.com; mmabdelh@ncsu.edu

Published online: 06 October 2009

The amplitude time characteristics of the deuteron beams were investigated in the Filippov type plasma focus [16]. A complex structure of the localized regions of generation of fast neutron in the MeV range in a plasma focus as a result of azimuthal destruction of the current sheath (CS) was observed experimentally [17]. Measurements of the X-ray energy flux was based on the explosive evaporation of the metal target [18]. The use of a Filippov type plasma focus machine as a pulsed intense source of hard X rays was evaluation [19]. A model has been presented for the description of behavior of the Filippov type plasma focus devices [20]. Some results of this model have been compared with experimental results of "Dena" Filippov type machine [20]. Another model also was used and based upon the slug model and Lee's model for Mather type PF devices [21]. On the other hand, a new model, "Masoud Model", has been developed to overcome the discontinuity between the axial phase and the radial phase in the plasma focus [22]. It is assumed that, according to the snow plow model, the plasma sheath in the radial phase moves in the angular direction with the continuity between the axial and the radial phases. This model is based on the introducing an angle of motion in all equations of motion and circuit. Then, the plasma sheath position and velocity were calculated numerically.

The spherical plasma focus device (SPF) is a special case between Mather and Filippov configurations. SPFs machines were suggested for the first time in Russian laboratories by Makeev et al. [23] in 1996 parallel with Egyptian researches in laboratories of the EAEA (Egyptian Atomic Energy Authority) in 1996.

The investigation chronology of devices with plasma focus was described in brief. The characteristics of several types of spherical chambers are given like that in Fig. 1. The applications of such devices as neutron and X-ray sources for the purposes of nuclear physics and engineering are outlined in the article. The perspective ways of plasma focus investigations, aimed to the solution of fundamental physical problems and its development for industrial technologies are shown [23].

A bright and reliable X-ray source for lithography has been developed using plasma focus. Discharge with constant pressure gas, one of the features of plasma focus, makes the X-ray source system simple and lengthens lifetime. A fine ceramic insulator made of alumina in place of a conventional Pyrex glass insulator improves the system reliability. The system operates for more than 10^5 discharges without maintenance. The lifetime of the system is ten times longer than that of a conventional plasma focus device. The resolution of a pattern printed by multi shot exposure depends not only on the diameter of pinched plasma but also on the variation of source position. A new spherical electrode surrounding the plasma-focusing space was added to stabilize the location of the spot on the axis by eddy currents which exert the Lorentz force on the plasma. The spot position deviation became negligibly small compared with the pinched plasma diameter [24].

The conventional tapered anode of the NX2 repetitive plasma focus device has been changed to two other shapes to investigate the effect of anode shape on neutron emission characteristics. However, the pressure at which the maximum neutron yield produced depends on the anode shape. The anode with spherical tip shows the most stable neutron emission with consistently good neutron yield and a single neutron peak energy was almost at all the filling gas pressures rather than the other anode shapes [25].

At Russia research institute of experimental physics (VNIIEF), a new type of PF chamber, the so called spherical PF chamber (SPFC), has been developed. The use of spherical electrodes made the chamber design more compact in comparison with Filippov and Mather chambers. Moreover, such an electrode system provides both the sufficiently long phase of plasma current sheath acceleration in the coaxial gap and the fast radial convergence of the sheath toward the axis [26]. For spherical PF chambers, the discrepancy between the simulation results and experimental data of the neutron yield is somewhat larger. The simulation geometry was similar to the geometry of the

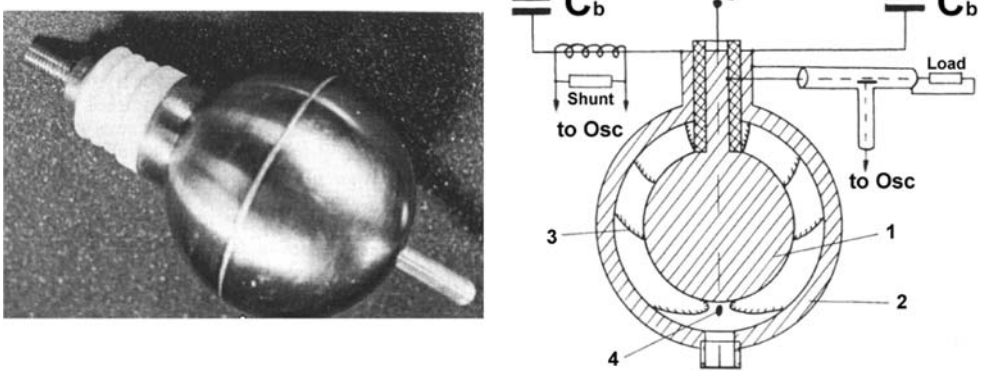

Fig. 1 Russian spherical plasma focus, C_b-condenser bank; *1*, anode; *2*, cathode; *3*, plasma sheath position in time; *4*, zone of PF formation

SFC-2 chamber. In the experiment, the initial deuterium pressure was 15 Torr, the maximum current was $\approx$0.8 MA, and the neutron yield was $\approx 3 \times 10^9$ neutrons. The calculated waveforms of the current time derivative and voltage at the chamber input were almost identical to the measured ones. The calculated neutron yield (without the after-focusing neutron tail) was $\approx 2.3 \times 10^9$ neutrons per shot, and the calculated duration of the neutron pulse was close to the measured one [26]. Although the total neutron yield calculated for the SFC chamber is close to the measured one, they did not achieve the calculation of the convergence on the neuron pulse duration and the neutron generation rate. The calculated duration of the neutron pulse was two times longer than the measured one. In simulations of plasma flows in curvilinear PF chambers, the required cell size of a rectangular mesh is much smaller than in simulations of Mather type PFs [26].

The aim of this study is to construct a simulation model which can describe the motion of plasma sheath between two concentric hemisphere electrodes. The plasma sheath velocity and temperature is to be calculated. The discharge current and voltage is to be drawn as a function of the discharge time. The results of this model are to be compared with other results of the other model that designed by Lee [4–14] for the cylindrical geometry.

Theoretical Aspects of the New Proposed Model

A new model has been developed for hemisphere electrodes. After breakdown, the rundown starts with plasma sheath lifting from the insulator surface followed by sheath motion under the influence of Lorentz force. The streaming velocity of the plasma is in the J $\times$ B direction [27]. The configuration used is shown in Fig. 2 where the discharge current J_r flows in the radial direction and the magnetic field B_Φ is in the azimuth direction so that the Lorentz force F_θ deflects the sheath to an angle θ. Then finally, the CS collapses forming the pinch, which is characterized by extremely high energy density and emission of intense radiation and high energy particles. It was shown that the luminosity of the plasma sheath as it propagates along the electrode in the PF devices was found to be produced mainly by the gas dynamic shock wave [28].

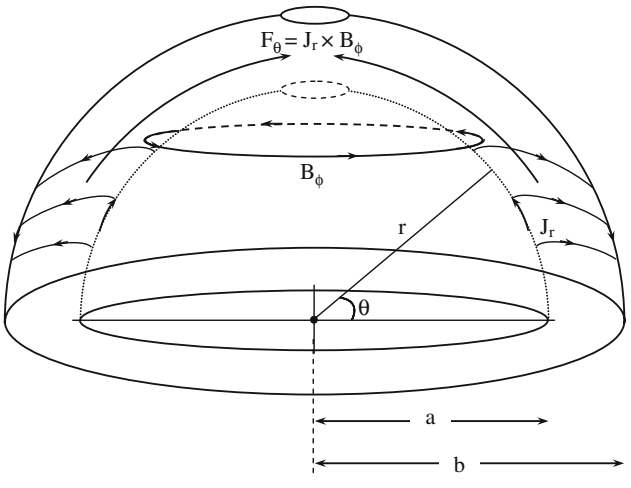

Fig. 2 Schematic diagram of the geometry and sheath motion in the SPF devices

Governing Equations

The discharge breakdown starts at the insulator forming a plasma sheath, then the snowplow model was applied to plasma sheath motion. Two equations are used during this phase: the equation of motion, which depends on the rate of the momentum change, and the circuit equation. By solving these two equations, we obtained the values of plasma parameters.

Equation of Motion

The force results from the rate of momentum change of the current sheath of mass m at position θ, is given by:

$$F_1 = \frac{d(mv_\theta)}{dt} = \frac{d(mr\dot{\theta})}{dt} = \frac{d}{dt}\left[\frac{2}{3}\rho f_m \pi (b^3 - a^3)\sin\theta r\dot{\theta}\right] \quad (1)$$

so that:

$$F_1 = \frac{2}{3}\rho f_m \pi (b^3 - a^3)\left[\sin\theta r\ddot{\theta} + r\dot{\theta}^2\cos\theta\right] \quad (2)$$

where b is the outer electrode radius, a is the inner radius, ρ is the initial gas density, v_θ is the tangential velocity, and f_m is the fraction of mass swept by the sheath motion. The mass factor is important to reduce the difference between the small value of the calculated velocity and the actual measured experimentally, due to the fact that the motion mass of the theoretical snowplow model is greater than the actual one [29]. The mass factor was investigated and found that it depends on the current value and the initial neutral gas density. The current density equation, the magnetic field in the form of Ampere's law, the equation of motion, and the energy stored in the system were used to calculate the mass factor [30].

The magnetic force F_2 exerted on the current sheath is:

$$F_2 = \int P\,dA = \int_a^b \frac{B^2}{2\mu} 2\pi r\cos\theta\,dr \quad (3)$$

where μ is the permeability of space, and the magnetic field B due to the current I at distance r is given by $\frac{\mu I f_c}{2\pi r\cos\theta}$ and f_c is the fraction of current flowing in the piston due to the

shedding effect in which some of the current is left behind the main current sheath [31]. The current factor is set in our experiment at value equal to 0.7. This factor is used for the shedding effect due to the fact that not all the current pass through the plasma sheath, but only about 70% is allowed and the other 30% passes through the insulator sleeve [32].

The magnetic pressure P in Eq. 3 is given by:

$$P = \frac{B^2}{2\mu} \tag{4}$$

And the area A equals to:

$$A = \int_a^b 2\pi r \cos\theta \, dr \tag{5}$$

so by using Ampere's law, one gets:

$$F_2 = \int_a^b \left[\left(\frac{\mu I f_c}{2\pi r \cos\theta} \right)^2 / (2\mu) \right] 2\pi r \cos\theta \, dr = \frac{\mu I^2 f_c^2}{4\pi \cos\theta} \ln\left(\frac{b}{a}\right) \tag{6}$$

The equation of motion is given by combining Eqs. 2 and 6 which gives:

$$\ddot{\theta} = \frac{d^2\theta}{dt^2} = \frac{\alpha I^2}{r \sin\theta \cos\theta} - \cot\theta \dot{\theta}^2 \tag{7}$$

where

$$\alpha = \frac{3\mu f_c^2}{8\pi^2 \rho f_m (b^3 - a^3)} \ln\left(\frac{b}{a}\right) \tag{8}$$

Circuit Equation

A simple equivalent electric circuit of the SPF device consists of a capacitor bank of capacitance C_o which is discharged through a circuit inductance L_o, stray resistance R_o, a switch, and the capillary tube. When the switch is closed, the charging voltage V_o is applied across the insulator. During the ignition, a breakdown occurs and an axial symmetric current sheath is formed. Then the current increases and the sheath moves towards the open end. Figure 1 shows a simple example of the electric circuit.

Ignoring the plasma resistance r(t), which is the approximation generally used for electromagnetic drive, then the circuit equation could be given by:

$$\frac{d}{dt}[(L_o + Lf_c)I] + r_o I = V_o - \int \frac{I\,dt}{C_o} \tag{9}$$

so,

$$(L_o + Lf_c)\frac{dI}{dt} + If_c\frac{dL}{dt} + r_o I = V_o - \int \frac{I\,dt}{C_o} \tag{10}$$

so,

$$\frac{dI}{dt} = \left[V_o - \frac{I\,dt}{C_o} - r_o I - I\beta\dot{\theta}\left(\frac{1 + \theta\tan\theta}{\cos\theta}\right) \right] \Big/ \left[L_o + \frac{\beta\theta}{\cos\theta} \right] \tag{11}$$

where

$$\beta = \frac{\mu(b-a)f_c}{2\pi} \tag{12}$$

In these equations, the plasma inductance was given by:

$$L = \int_a^b \frac{\mu r\theta}{2\pi r \cos\theta} dr \tag{13}$$

So that

$$L = \frac{\mu(b-a)\theta}{2\pi\cos\theta} = \frac{\beta\theta}{\cos\theta} \tag{14}$$

hence

$$\frac{dL}{dt} = \beta\dot{\theta}\sec\theta(1 + \theta\tan\theta) \tag{15}$$

The Discharge Voltage

The discharge voltage across two hemispheres terminals of SPF device could be calculated using the flowing equation:

$$V = \frac{d}{dt}(LIf_c) = f_c I\frac{dL}{dt} + f_c L\frac{dI}{dt} \tag{16}$$

hence

$$V = \frac{\beta f_c}{\cos\theta}\left[\theta\frac{dI}{dt} + I\dot{\theta}(1 + \theta\tan\theta)\right] \tag{17}$$

Using Eqs. 7, 11, and 14, the plasma sheath motion can be described.

$$\text{at } t = 0, \theta = 0, \dot{\theta} = 0, I = 0, I\,dt = 0, \frac{dI}{dt} = \frac{V_o}{L_o},$$

$$\ddot{\theta} = \frac{\alpha}{r}\sqrt{\frac{2}{3}\frac{V_o}{L_o}}$$

Next step values are computed using the following linear approximations:

$$\begin{aligned} \frac{d\theta}{dt} &= \frac{d\theta}{dt} + \frac{d^2\theta}{d^2t}D \\ \theta &= \theta + \frac{d\theta}{dt}D \\ I &= I + \frac{dI}{dt}D \\ \int I\,dt &= \int I\,dt + ID \end{aligned} \tag{18}$$

Increment time, D, is added again and repeat the calculations of next step to generate the new values. Continue procedure until $\theta = 85°$.

Shock Wave Velocity and Plasma Temperature Equations

From slug model, which is suitable for modeling a plasma focus, the magnetic pressure drives a shock wave, creating a space for the current sheath of the magnetic piston to move into. According to the shock wave theory, the shock wave velocity is given by [4]:

$$v_s = \frac{dr_s}{dt} = -\left[\frac{\mu(\gamma+1)}{f_m \rho}\right]^{1/2} \frac{If_c}{4\pi r \cos\theta} \quad (19)$$

where γ is the specific heat ratio.

From the shock wave relation, the plasma temperature T is given by [5, 33]:

$$T = \frac{M}{R_o D} \frac{2(\gamma-1)}{(\gamma+1)^2} v_s^2 \quad (20)$$

where: R_o is the universal gas constant, M is the molecule weight, D_N is the dissociation number; Z_{eff} is the effective charge of the plasma. For example for deuterium $D_N = 2$, whereas for Argon $D_N = 1$.

Results and Discussion

In this study, we will investigate the differences between various results that could be obtained from the simulation of the SPF as compared to that of the classical cylindrical plasma focus devices. The results will be carried out for the same charging voltage, capacity of condenser bank, circuit inductance, circuit resistance, gas type and pressure, and the same electrodes radii of both the cylindrical and the spherical systems. The output results include the discharge current, discharge voltage, sheath velocity and position, and plasma temperature.

The system consists of two concentric hemispheres of 1.05 cm radius for the outer electrode and 0.8 cm radius for the inner electrode. In the case of the cylindrical geometry, the radii are the same as that of the spherical geometry with 1 cm length of the inner electrode. The charging voltage is 25 kV which is used to charge a capacitor of 0.16 μF and discharge it through circuit inductance of 65 nH. The working gas is the hydrogen with pressure of 0.36 torr. The system geometry and circuit components values were chosen to be similar to that of the experiment of Moreno et al. [34].

Figure 3 shows a comparison between the discharge currents as a function of the discharge time which was calculated for both cylindrical and spherical structures. It is shown that the dip current at 0.2 μs in case of the spherical devices is deeper than that of the cylindrical devices. The thick lines in this figure and all next figures refer to the cylindrical device while the thin lines refer to the spherical device.

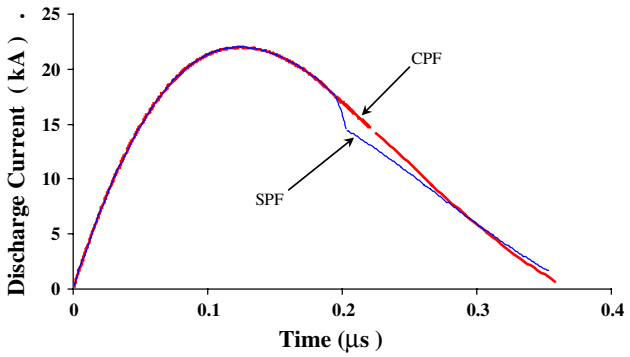

Fig. 3 Discharge current as a function of the discharge time

The variation of the discharge voltage as a function of the discharge time is shown in Fig. 4. This figure shows that the spike voltage at 0.2 μs for the spherical device is expected to be sharper and higher than that of the is cylindrical device. The current dip and the voltage spike are evidences of focusing in plasma focus devices [2, 4]. The higher voltage spike and deeper current dip could result in better focusing conditions. Equation 17 shows that the discharge voltage is directly proportion with the rate of change of the discharge current in Eq. 11. So, due to the higher change of the discharge current, dI/dt of the spherical system, as that for the current dip in Fig. 3, then the voltage spike is expected to be higher as in Fig. 4.

Figure 5 shows the plasma velocity variation as a function of the discharge time for both the cylindrical and the spherical devices for the same discharge current and circuit properties. It is shown that the axial speed of the plasma current sheath in the cylindrical devices tends to saturate at the end of the inner electrode after about 130 ns at which the motion of the plasma current sheath is deflected to the radial direction. But for the spherical devices, the variation of the plasma sheet direction occurs directly from the beginning of the sheet creation at the sleeve. This is due to the configuration shape of the spherical device.

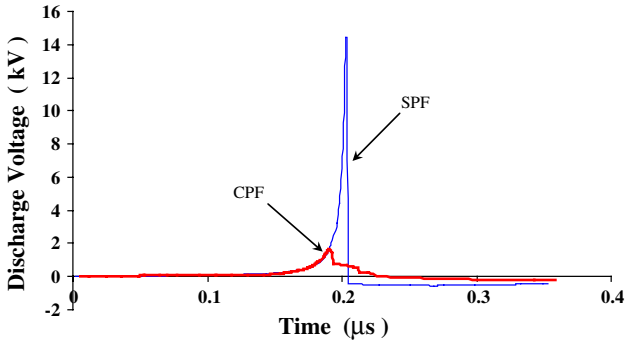

Fig. 4 The discharge voltage as a function of the discharge time

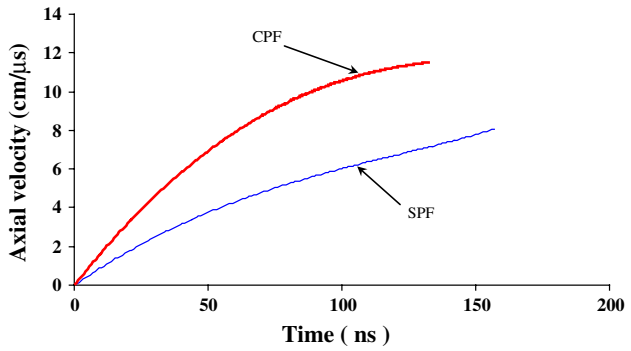

Fig. 5 A comparison between the axial velocity of the CS and SW as a function of the discharge time in both cylindrical and spherical systems

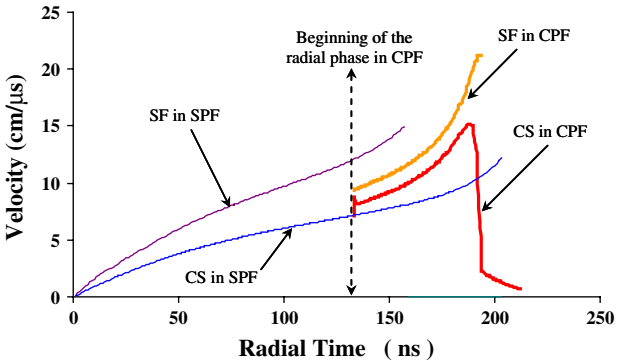

Fig. 6 A comparison between the CS and SW velocities as a function of the discharge time in both cylindrical and spherical systems

Figure 6 shows the differences between the plasma current sheet (CS) velocity in the spherical plasma focus (SPF) and the radial velocity in the cylindrical plasma focus (CPF) devices. The figure shows also the behaviour of the shock front (SF) velocities in both configurations. The formation of a stabilized shock wave depends mainly on the discharge conditions, and especially on the initial rate of current increase [35]. In particular, for shock tubes of large radius ratio, the magnetic pressure may decrease by orders of magnitude across the annulus, thus, it cannot be balanced by the dynamic pressure [36].

It is shown in Fig. 6 that the velocities of the CS and SF are higher in the case of the CPF devices as compared to that of SPF. Equation 7 shows that such behaviour could be expected since the acceleration and in turn, the velocity directly depends on the discharge current. Because the discharge current shows a faster decreasing for the spherical devices as compared to the cylindrical one as shown for deeper current dip in Fig. 3, hence the velocity is expected to be lower in the spherical devices.

The radial position of CS and SF are shown in Fig. 7 for both the cylindrical and the spherical devices. In case of the cylindrical devices, the shock wave needs about 67 ns from

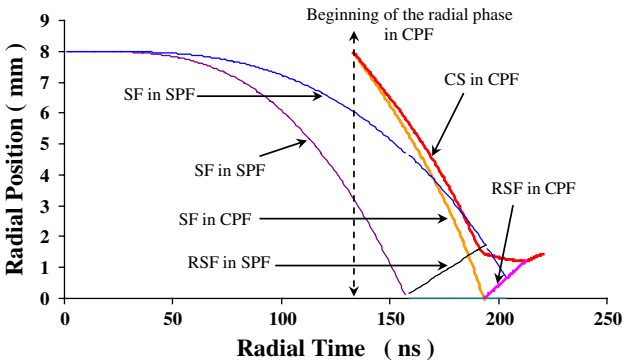

Fig. 7 A comparison between the CS and SW position as a function of the discharge time in both cylindrical and spherical systems

beginning of the radial motion to hit the axis, creating a reflected shock front (RSF). While for the spherical devices, the reflected shock takes place after about 157 ns from the start of the discharge. In this model, joule heating gain term, the line radiation and Bremstrahlung loss terms are not taken into account during this study.

The plasma temperature is shown in Fig. 8 for the cylindrical and the spherical geometries. The figure shows that the plasma temperature for the spherical device is expected to be lower than that for the coaxial one. The plasma temperature is calculated depending on the shock wave velocity as in Eq. 19. So, due to the lower value of the shock wave velocity in the spherical devices as compared to that of the coaxial devices as shown previously in Fig. 6, hence the plasma temperature is also expected to be lower in the spherical devices.

The plateau part in the upper side of both temperature curves is due to a constant shock speed. When the inward radial shock hits the axis, in the computation, the reflected shock phase begins. The code used a constant reflected shock speed v_{rs}, of 0.3 of on-axis inward radial shock speed ($v_{rs} = 0.3\ v_s$) [37]. This value is checked for many plasma focus experiments of several geometries and under variant conditions which gave good fitted results. The decrement of plasma temperature after that is due to the lower

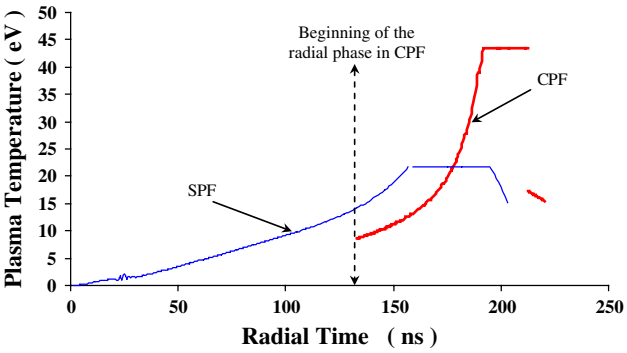

Fig. 8 Plasma temperature as a function of the discharge time

discharge current hence lower input energy. The decrement could also be referred to the line radiation and Bremstrahlung loss terms [8, 9], but both of them are not taken into consideration during this study.

Conclusion

In this study, we have simulated plasma pinch of hemisphere devices. The motion of plasma sheath between two hemisphere electrodes was described using snow plow model. The current dip and voltage spike as a result of creation of plasma focus was obtained depending using a simple circuit equation. In the hemispherical device, the current dip was deeper and voltage spike was higher than that in the cylindrical one. The equation of motion according to the rate of the momentum change enabled us to obtain the plasma sheath velocity, sheath position, and plasma temperature. It was found that the plasma sheath velocity and temperature in the case of the cylindrical system were higher than that in the spherical one.

The applied snowplow model could be used to describe the plasma motion for the spherical devices. The plasma energy gain from joule heating and the loss terms due to line radiation and Bremstrahlung could be applied in future in order to get more accurate results about the plasma temperature and plasma sheath velocity.

Acknowledgments The author would like to thank Prof. Dr. M. M. Masoud (Plasma Physics Department, Atomic Energy Authority AEA, Egypt) and Prof. Dr. M. Bourham (Nuclear Engineering Department, NCSU, USA) for their kind support and useful discussions.

References

1. J.W. Mather, *Plasma Physics, Methods of Experimental Physics*, vol. 9B (Academic Press, New York, 1971), p. 187
2. J.W. Mather, Phys. Fluids **7**, S28 (1964)
3. N.V. Filippov, T.I. Filippova, V.P. Vinogradov, Nucl. Fusion Suppl. **2**, 577 (1962)
4. S. Lee, in *Proceedings of the first Tropical College on Applied Physics: "Laser and Plasma Technology"*, Malaysia, Kuala Lumpur, (1985), p. 387
5. S. Lee, in *Proceedings of the first Tropical College on Applied Physics: "Laser and Plasma Technology"*, Malaysia, Kuala Lumpur, (1985), p. 3
6. S. Lee, in *Proceedings of the first Tropical College on Applied Physics: "Laser and Plasma Technology"*, Malaysia, Kuala Lumpur, (1985), p. 37
7. S. Lee, C.S. Wong, T.Y. Tou, J.B. Jalil, A.C. Chew, in *Proceedings of the first Tropical College on Applied Physics: Laser and Plasma Technology*, Malaysia, Kuala Lumpur, (1985), p. 63
8. B. Shan, P. Lee, S. Lee, Sing. J. Phys. **16**, 25 (2000)
9. M.H. Liu, S. Lee, in *Proceedings of 1998 ICPP & 25th EPS Conference Controlled Fusion and Plasma Physics*, Praha, vol. 22C, (1998), p. 2169
10. S. Lee, A. Serban, IEEE Trans. Plasma Sci. **24**, 1101 (1996)
11. S. Lee, J. Appl. Phys. **54**, 3603 (1983)
12. S. Lee, S.H. Saw, Appl. Phys. Lett. **92**, 021503 (2008)
13. S. Lee, S.H. Saw, J. Fusion Energ. **27**, 292 (2008)
14. S. Lee, P. Lee, S.H. Saw, R.S. Rawat, Plasma Phys. Control. Fusion **50**, 065012 (2008)
15. S. Lee, S.H. Saw, P.C.K. Lee, R.S. Rawat, H. Schmidt, Appl. Phys. Lett. **92**, 111501 (2008)
16. N.V. Filippov, T.I. Filippova, JETP Lett. **29**, 689 (1979)
17. N.V. Filippov, I.V. Kurchatov, JETP Lett. **31**, 120 (1980)
18. N.V. Filippov, T.I. Filippova, I.V. Khutoretskaia, V.V. Mialton, V.P. Vinogradov, Phys. Lett. A **211**, 168 (1996)
19. N.V. Filippov, T.I. Filippova, M.A. Karakin, V.I. Krauz, V.P. Tykshaev, V.P. Vinogradov, Y.P. Bakulin, V.V. Timofeev, V.F. Zinchenko, J.R. Brzosko, J.S. Brzosko, IEEE Trans. Plasma Sci. **24**, 1215 (1996)
20. S. Goudarzi, R. Amrollahi, R.S. Moghaddam, J. Fusion Energ. **27**, 195 (2008)
21. V. Siahpoush, M.A. Tafreshi, S. Sobhanian, S. Khorram, Plasma Phys. Control. Fusion **47**, 1065 (2005)
22. M.M. Masoud, H.A. El-Gamal, H.A. El-Tayeb, M.A. Hassouba, M.A. Abd Al-Halim, Plasma Devices Oper. **15**, 263 (2007)
23. N.G. Makeev, V.G. Rumyantsev, G.N. Cheremukhin, *Physics and Engineering of Pulse Sources of Ionizing Radiations for Investigation of Fast Processes*, Sarov, (1996), p. 281 (in Russian)
24. Y. Kato, I. Ochiai, Y. Watanabe, S. Murayama, J. Vac. Sci. Technol. B **6**, 195 (1988)
25. F. Malik, S.M. Hassan, R.S. Rawat, M.V. Roshan, T. Zhang, S. Mahmood, J.J. Lin, T.L. Tan, P. Lee, H. Schmidt, S.V. Springham, in *Pulsed Power Conference, 16th IEEE International*, vol. 2, p. 1703, 17–22 June 2007
26. S.F. Garanin, V.I. Mamyshev, Plasma Phys. Rep. **34**, 639 (2008)
27. J. Marshall, I. Henins, Los Almos, Nucl. Fusion, **2**, (1960). Published by the International Atomic Energy Agency, Vienna, 449 (1966)
28. T.D. Butler, I. Henins, F.C. Johada, J. Marshall, R.L. Morse, Phys. Fluids **12**, 1904 (1969)
29. N.F. Tsagas, G.L.R. Mair, A.E. Prinn, J. Phys. D: Appl. Phys. **11**, 1263 (1978)
30. G.L.R. Mair, N.F. Tsagas, A.E. Prinn, Phys. Lett. A **58**, 315 (1976)
31. S.P. Chow, S. Lee, B.C. Tan, J. Plasma Phys. **8**, 21 (1971)
32. H. Bhuyan, S.R. Mohanty, N.K. Neog, S. Bujarbarua, R.K. Rout, Meas. Sci. Technol. **14**, 1769 (2003)
33. K.H. Kwek, T.Y. Tou, S. Lee, IEEE Trans. Plasma Sci. **18**, 826 (1990)
34. J. Moreno, P. Silva, L. Soto, Plasma Sources Sci. Technol. **12**, 39 (2003)
35. C.T. Chang, Phys. Fluids **4**, 1085 (1961)
36. J.C. Keck, Phys. Fluids **5**, 630 (1962)
37. V. Siahpoush, M.A. Tafreshi, S. Sobhanian, S. Khorram, Plasma Phys. Control. Fusion **47**, 1065 (2005)